materials

MDPI

Article

Enhancement of mechanical properties of pure aluminium through contactless melt sonicating treatment

Agnieszka Dybalska[1,*], Adrian Caden[1], William D. Griffiths[1], Zakareya Nashwan[1], Valdis Bojarevics[2], Georgi Djambazov[2], Catherine E.H. Tonry[2] and Koulis A. Pericleous[2]

[1] School of Metallurgy and Materials, University of Birmingham, Birmingham B15 2TT, UK; A.Dybalska@bham.ac.uk (A.D.); J.A.Caden@bham.ac.uk (A.C.); W.D.Griffiths@bham.ac.uk (W.D.G.); ZSN584@student.bham.ac.uk (Z.N.)

[2] Centre for Numerical Modelling and Process Analysis, University of Greenwich, London SE10 9LS, UK; v.bojarevics@gre.ac.uk (V.B.); g.djambazov@gre.ac.uk (G.D.); C.Tonry@gre.ac.uk (C.T.); k.pericleous@gre.ac.uk

* Correspondence: dybalska.ag@gmail.com

Abstract: A new contactless ultrasonic sonotrode method has been designed to provide cavitation conditions inside liquid metal. The oscillation of entrapped gas bubbles followed by their final collapse causes extreme pressure changes leading to de-agglomeration and dispersion of oxide films. Forced wetting of particle surfaces and degassing are other mechanisms thought to be involved. Previous publications showed a significant decrease in grain size using this technique. In this paper, the authors extend their study to strength measurements, demonstrating an improvement in cast quality. Degassing effects are also interpreted to illustrate the main mechanisms involved in alloy strengthening. Mean values and Weibull analysis are presented where appropriate to complete the data. The test results on cast Al demonstrate a maximum of 48% grain refinement, 28% increase in elongation compared to 16% for untreated material and up to 17% increase in ultimate tensile strength (UTS). Under conditions promoting degassing, the hydrogen content was reduced by 0.1cm^3/100g.

1. Introduction

The metal casting industry and academic communities are extremely interested in improving melt quality. The microstructural refinement can be achieved, for example, by gating system optimization or melt inoculation [1-3]. Another promising route is the ultrasonic treatment (UST) of liquid metal. This method provides alloys with degassing, filtration and grain refinement [4-8]. Instead of the traditional immersed sonotrode, the contactless electromagnetic probe has been recently developed to avoid melt contamination, by probe damage due to corrosion in more reactive melts and to treat larger volumes of metal [9-11].

During processing, pressure vibrations induced in the melt by an external induction coil lead to acoustic resonance in the liquid alloy. This leads in turn to the oscillation of entrapped gas bubbles followed by their eventual collapse, the phenomenon of cavitation. Cavitation requires an ultrasonic pressure intensity larger than the cavitation threshold [5,6] and its presence is desirable in the melt as it leads to beneficial changes in the finished product. .

The first observed benefit is that of degassing [5,6,12,13]. Usually in molten metal, some dissolved gases are present, for example, we can expect the presence of hydrogen

in aluminium due to its high solubility [14]. Gas bubbles are formed on nucleation sites (for example oxide particles) and grow by diffusion of dissolved gas from the melt into the bubble. In a solidified casting bubbles become pore defects reducing the strength of the metal. In the presence of ultrasound bubbles oscillate in size, in response to the changing acoustic pressure in the liquid. The bubbles' behaviour in the sound field is governed by the Bjerknes forces [15]. Those forces move the bubbles up or down the pressure gradient created by the sound waves, or cause them to accumulate at pressure nodes [15]. As a result, the bubbles that have not collapsed can coalesce and due to buoyancy float to the surface where the hydrogen is released into the atmosphere.

The second benefit is that of structure refinement. In the right conditions the bubbles will not only oscillate but finally collapse. This event leads to extreme local pressure changes due to the shock waves and high-speed jets produced [5,6,16]. Such pressure changes are expected to be large enough to cause mechanical stress in intermetallic crystals or oxides, causing fragmentation by cracks due to brittle fracture [17]. After de-agglomeration, dispersion occurs. In addition to these local high-speed jets, the whole volume of metal is also stirred. The source of stirring is the time-averaged Lorentz force induced in the melt by the electromagnetic field generated by the contactless sonotrode [10]. The flow will disperse the de-agglomerated particles that can then serve as nucleation sites facilitating heterogeneous crystallization [7,18-21]. This process is commonly known as the "activation" of impurities where the combined effect of dispersion and forced wetting, due to pressure differences in the liquid [5-7]. Finally, emerging crystals can also be broken by the shock waves reducing the grain sizes [5-7,22]. Under sonication, the growth of dendrites will be restricted, assisting equiaxed growth. Note, as we treat the metal prior to solidification in the experiments shown here, this effect is less significant.

The improvement of the metal microstructure caused by contactless ultrasonication has been systematically reported [10,11,23-26]. The Hall-Petch equation [27] predicts that as the grain size decreases, the Yield Strength increases. Also, the strength is reduced by the porosity [14]. As a consequence, reduction of the grain size and gas content due to ultrasound treatment result in metal strengthening. Previously observed grain size reduction occurred in pure aluminium and alloys inoculated by a grain refiner introduced, in quantity below that commercially used, to assist the heterogeneous cavitation [10,11,23-26].

To check the metal quality, the Yield Strength (YS) or Ultimate Tensile Strength (UTS) and percentage elongation (L%) are commonly found by testing metal samples. Statistically, the fracture is described by the Weibull distribution based on the weakest link theory [27, 28]. The cumulative probability function of the two-parameter Weibull distribution is therefore expressed as follows (equation 1):

$$P = 1 - \exp\left[-(\sigma \, \sigma_0^{-1})^m\right], \tag{1}$$

where P is the probability of failure at a given property (stress, strain, fatigue life, etc.), σ, or lower. The parameter σ_0 is a distribution scale parameter, and m is the shape parameter. The shape parameter is also known as the Weibull modulus, a parameter that reflects how much the data are scattered, with a higher Weibull modulus meaning a lower probability of fracture under stress. This approach has been adapted for metallurgy and has been widely used [29-31]. The Weibull modulus, established from the tensile strength for gravity-filled castings, is generally thought to range between 10 and 30. For aerospace castings, it is expected to be between 50 and 100 [32]. For example, it is about 73.8 for a ductile steel 1018 and 91.4 for an aluminium alloy AL 7075-T651 and can be as high as 124.0 observed for Al 6061-T651 alloy [33].

This paper shows recent tensile test results (UTS and elongation) of ultrasonicated metal, demonstrating improvement in cast metal quality. Degassing effects and microstructure refinement are interpreted to analyse the main mechanisms involved in alloy strengthening.

2. Materials and Methods

Casting experiments were conducted in a cylindrical clay-graphite crucible with an external diameter of 170 mm, an internal diameter of 135 mm and a height of 320 mm. For each experiment, the crucible was filled with about 8.5 kg metal, commercial purity aluminium (CP-Al) with the addition of 0.15 wt.% Al-5Ti-1B grain refiner to increase the potential number of nucleation sites for cavitation. The amount of grain refiner is small enough to make changes in the microstructure easily observable. The prototype "top-coil" (a "first generation" contactless sonotrode)[9-11] was used for the sonication of the liquid metal. During processing, the ambient ultrasonic noise emitted around the crucible was recorded by an Ultramic®200K (Dodotronic, Castel Gandolfo, RM, Italy) digital ultrasonic microphone. The recorded sound was observed in the form of an FFT (Fast Fourier Transform) sound spectrum extracted in real-time during experiments using MATLAB® (MathWorks, Natick, MA, USA) software. The broadband noise emitted by collapsing bubbles [23,34] acted as an indicator of the presence of cavitation. Broadband noise was seen as light-coloured vertical lines on spectrograms recorded under varying conditions. The lines were normal to the continuous horizontal lines denoting the top-coil frequency signal, observed at around 20 kHz, and the induction furnace signal, observed at around 5 kHz. Cavitation was seen to be intermittent, and the number and density of vertical lines was considered to be a good indication of cavitation activity [23,35].

Where broadband noise was observed, the process conditions (coil frequency, melt temperature) responsible for the noise were maintained and at least 1-2 minutes of processing was recorded and presented on the spectrograms. In some cases, the local conditions in the setup resulted in near-resonant conditions in the crucible, where bubbles could oscillate continuously at their own resonant frequency but did not implode. By 'local conditions' we mean the parameters such as melt volume, or the off-axis position of the crucible relative to the top-coil head, and others. When that happened, only degassing was observed. Results of that degassing were compared with processing followed by grain size change. In each case, after 4-5 minutes of processing, samples were taken using the KBI ring test [36]. For this test, the liquid metal is poured into a steel ring with an outside diameter of 75 mm, inside diameter 50 mm and height of 25 mm placed on an insulating silica brick. Usually, the mass of aluminium samples is 70-100 g. To characterize the grain size, the base of the cylindrical samples were removed to about 3 mm above the base and ground, polished and etched with either Poultons' or Kellers' solution. The average grain size was then determined by the mean linear intercept method after taking photographs using a Zeiss Axioskop 2 (Zeiss, Oberkochen, BW, Germany) microscope equipped with an AxioCam HRc camera (Zeiss, Oberkochen, BW, Germany). To show the samples with a larger magnification, the standard microstructure photographs were taken by a Fuji camera (Fujifilm, Minato CITY, Tokyo, Japan) with optical zoom.

Following the KBI ring test, a second sample was poured into a Severn Science Gas Analyser (MechaTech Systems Ltd, Thornbury, Bristol, UK) to determine the hydrogen content. The remainder of the processed metal was poured into a sand mould (See Figure 1) in order to obtain tensile test-bars which were later machined to the size required for the tensile strength tests.
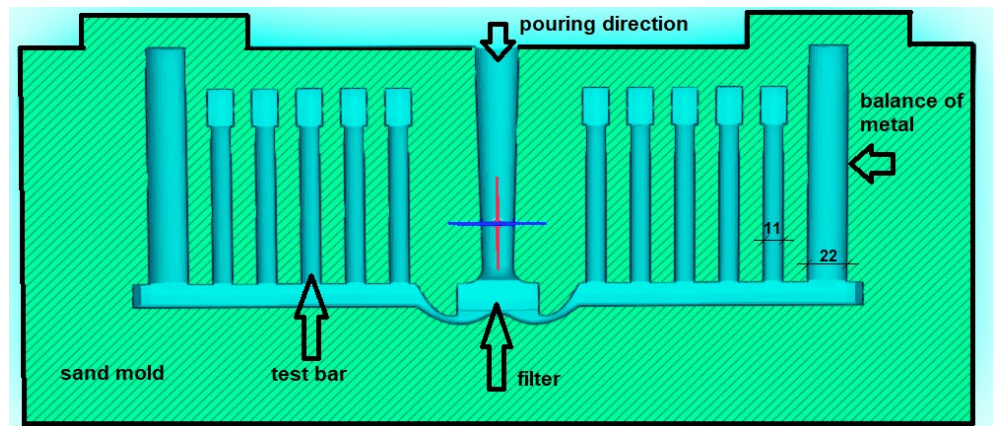
Figure 1. The draft of the sand mould used for casting of 10 test-bars for tensile strength tests. Two crucial diameters are given in mm, the sketch scale is 1:1. Liquid metal is poured into the mould from the top opening, it passes the filter and feeds the 10 test-bars cavities (diameter 11 mm). The higher cavities on both ends (diameter 22 mm) balance the pressure to feed the mould correctly.

In each experiment one mould was cast and 10 tensile specimens were produced. Producing more than 10 test-bars in one experiment is difficult due to the low initial temperature used. It is easier to release dissolved hydrogen from the melt at lower temperatures, hence the cavitation intensity decreases with the temperature increase and almost disappear at 720°C. Thus, the processing happened at 710°C. That low temperature shortened the time frame for casting into the mould. Due to fluidity loss with time, filling two moulds was tough.

The cast metal was filtered using a 20 ppi filter to avoid the presence of excessive oxide films. The process was repeated without ultrasound processing, to obtain reference test-bars. In that case, instead of the ultrasonic processing, the liquid metal was left inside the induction furnace, at the same temperature as before, for the time usually required for the contactless sonotrode treatment. Both the reference and processed samples were tested with an applied strain rate of 1 mm/min by the Zwick/Roell Z030 Universal Mechanical Tester (Zwick Roell Group, Ulm, BW, Germany), equipped with a micro-extensometer.

The data obtained were analysed with the help of scripts in Matlab and R-Studio software. To establish the Weibull modulus by the linear regression method [37-40], unbiased estimators were used following the approach described in [37] depending on the sample size (n - number of measurements). The general form of the estimator used in that procedure was (equation 2):

$$P = (i-a)(n+b)^{-1}, \qquad (2)$$

where i is the rank of the data point in the sample in ascending order, n represents the sample size, and a and b are numbers specific for the sample size found by the computer simulation [37].

For a sample size n=20 that estimator is in the form (equation 3):

$$P = (i-0.417)(n+0.030)^{-1}, \qquad (3)$$

while for n=10 it is (equation 4):

$$P = (i-0.348)(n+0.190)^{-1}. \qquad (4)$$

Where other estimators were used, the estimator form has been given in the text. The coefficient of determination (R^2) for each regression line is also presented.

The error was estimated by the simulation in Matlab. The Weibull modulus M' has been found by linear regression after sampling 10 or 20 unique and random values from the distribution with the chosen shape parameter m=M. This procedure was repeated 50000 times and the mean value and the standard deviation of the mean were extracted. The ratio of M' (found from 10 or 20 values) and Weibull modulus M set as a "true" value in the program, is treated as the bias of the method [compare: 38].

3. Results

3.1. Grain refinement after sonication

Experiments denoted 1 and 2 are the principle results in this paper. The effect of the first treatment (Experiment 1) is presented below in Figure 2. The grain size of a processed metal (b,d) is compared with the initial grain size observed in the untreated metal (a,c). As can be seen in the image without microscopic magnification (c,d) the grain size decreased strongly. From the photographs taken in the microscope a decrease is of about 48% from the initial size. The exact grain sizes are given in Figure 2.
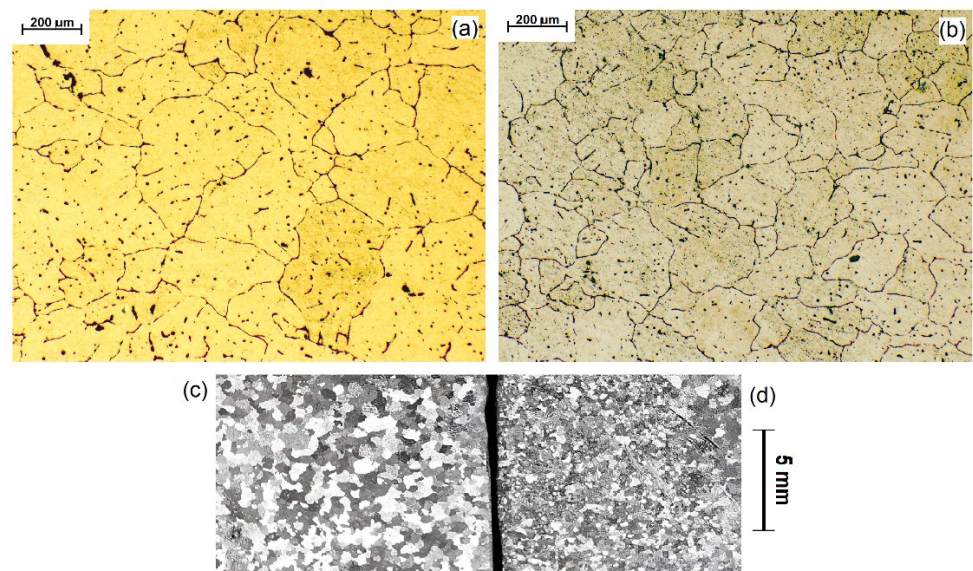

Figure 2. Experiment 1: (a) The grain size of untreated metal (208±38 μm) and (b)after treatment (108±19 μm) decreased by 48%, which is clearly indicated by a macro-scale photograph of a sample taken (c) before and (d) after ultrasonication.

In the next experiment (denoted experiment 2) another set of test-bars was cast and the grain sizes of the metal before and after treatment have been presented in Figure 3. The initial grain size was similar to the previously prepared reference set (Figure 2 c). In this case the grain size decreased by about 28% from that value.
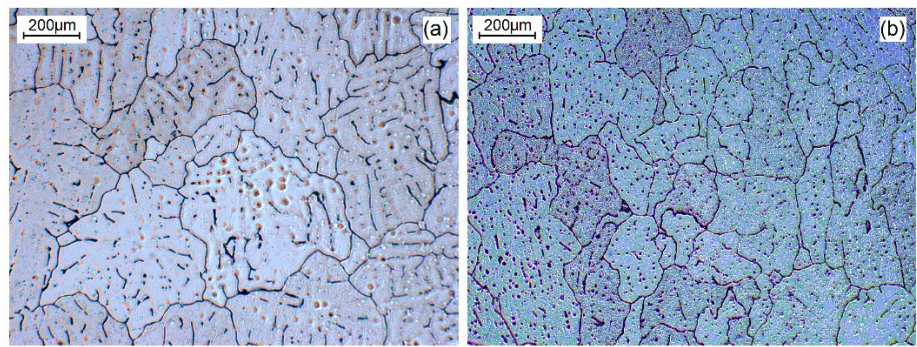
Figure 3. Experiment 2: (a) The grain size of untreated metal (204±13 μm) and (b) after treatment (147±4 μm) decreased about 28%.

The decrease in grain size is the effect of metal ultrasonication, which appears to be less effective in this case. The contactless sonotrode frequency is set in near–resonance conditions, unique for each experiment. The spectrograms of the sound recorded near the crucible indicated the extent of cavitation during both experiments, and are shown in Figure 4.
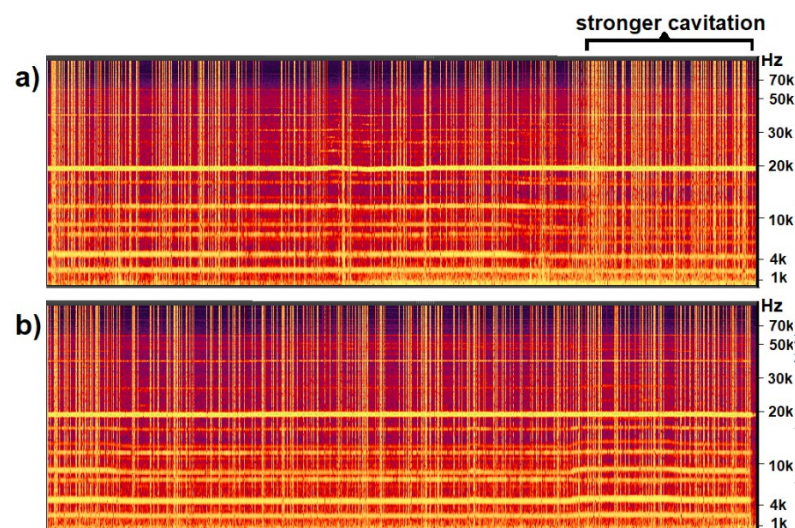

Figure 4. Spectrograms extracted from the recorded sound: (a) experiment 1, ultrasonication with frequency 18.86 kHz, (b) experiment 2, ultrasonication with frequency 18.42 kHz. The time of recording in both cases is about 5 minutes long.

The vertical light lines, perpendicular to the sonotrode signal seen as a horizontal line at 20 kHz, can be treated as an indication of cavitating bubbles [23, 34]. In both cases, almost all the treatment time was recorded. In the first experiment, we see that the cavitation intensity seems to be higher at the end of the process. This could be an explanation as to why the grain size in this experiment decreased by 48%, while in the second case, the decrease was only 28%. It is not unusual for the effect to be different in each experiment. The cavitation intensity depends on local conditions, including liquid volume, temperature, crucible position, crucible wall material and etc. as is the frequency that causes the resonance [34]. For industrial use keeping those conditions constant would be possible in a specially designated set-up; using a feedback mechanism, but in this experimental set-up it is difficult. Each experiment is therefore unique and the

near-resonant frequency is found in real-time by the operator observing the FFT of the
recorded noise. Thus, the cavitation intensity differs in individual treatments and the
observed grain size reflects that intensity.

3.2. Gas content decrease due to sonication

In both the experiments presented above, the degassing potency of the contactless
sonotrode was determined. The gas content before and after processing is given in Table
1 and compared with results of similar experiments in which only the degassing level
was determined. Two experiments described before, in which test-bars were produced
(Figures 2-4), are labelled as Ex1 (experiment 1) and Ex2 (experiment 2) in this paper.

Table 1. Degassing achieved by contactless ultrasound treatment.

	Fre-quency [kHz]	Tem-pera-ture [°C]	Gas content before treat-ment [cm^3/100g]	Gas content after treat-ment [cm^3/100g]	Gas content decrease [cm^3/100g]	Gas content decrease [%]
Ex1	18.86	710	0.17	0.11	0.06	35%
Ex2	18.42	710	0.16	0.12	0.04	35%
Ex3	18.61	706	0.17	0.11	0.06	35%
Ex4	18.32	700	0.15	0.04	0.11	73%
Ex5 (*)	18.42	709	0.20	0.14	0.06	30%

(*) degassing only - no grain refinement produced

Both experiments (Ex1 and Ex2) were accompanied by a decrease in gas content of
about 0.05 cm^3/100 g. As can be seen in the example of experiment Ex4, the degassing can
be much stronger. The maximum change (Ex4) of the gas content was about two times
greater than in experiments Ex 1-3. Slightly less of a degassing effect in Ex2 than in Ex1
can be associated with a smaller cavitation intensity, manifested by a smaller grain re-
finement effect (compare with Figures 2-4).

Previously examples of reported gas content decrease due to traditional ultrasound
processing, has been from 0.35 to 0.17 cm^3/100g [13], a reduction of 50%. In experiment 4
the gas content decreased 3.75 times. Unfortunately, the alloy used in [13] and the pro-
cessing conditions were different, but the efficiency of the contactless sonotrode in de-
gassing seems to be at least comparable.

To summarise, results presented show that contactless sonication provides: (I) grain
refinement, (II) degassing.

The open question then is, how does the ultrasound treatment improve the strength
of processed metals? As mentioned in the introduction, both effects – the grain size de-
crease and the gas content reduction should improve the cast metal quality. To determine
how the described changes influenced the strength of the alloy in Ex1 and Ex2, in which
elongation and UTS were measured. In Table 2 the mean values of elongation before and
after treatment have been given.

3.3. Elongation after sonication

Table 2. Mean elongation before (L) and after (L') treatment.

3	L[%] reference	L'[%] after treatment	L'/L	L'/L [*100%]
Ex1		27.5 ± 6.5	1.73	173%
Ex2	15.9 ± 3.0	24.2 ± 4.2	1.52	152%
Ex5 (*)		15.5 ± 6.5	0.98	98%

(*) degassing only, no grain refinement

The mean elongation after treatment is 52-73% greater than that observed for the same alloy without sonication. The results are consistent with previous findings – in experiment 1 we previously observed greater grain size decrease and slightly more degassing than in experiment 2. This was followed by better metal quality. In comparing with the degassed only samples (Ex5) the assumption can be made that the degassing at this level plays a negligible effect so that the main mechanism in the improvement is associated with the grain size decrease. Aluminium belongs to the class of ductile materials and an improved elongation is important for future applications of the metal.
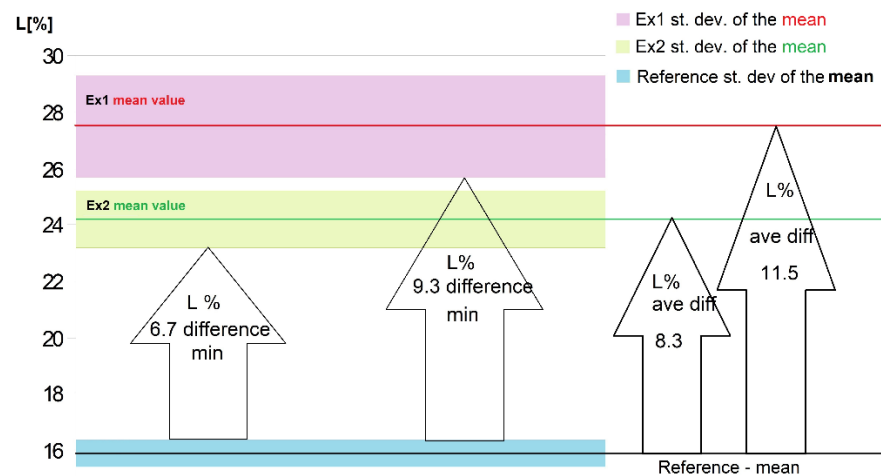

Figure 5. Measurements of elongation – the mean values and the error found in each experiment. The arrows show the minimum differences between elongation with and without treatment (difference min) or the difference between mean values (ave diff).

As mentioned before, each unique experiment produced a casting of 10 test-bars. For the reference set, the temperature history of the melt was repeated and we were able to produce equivalent tensile specimens. Thus, the reference values of both (UTS and elongation) tests are established from 20 results. As expected, the observed error is smaller in that case than for experiments Ex1 and Ex2, when only 10 specimens were tested, as can be seen in Figure 5.

Even taking into account the error shown in Figure 5, both measured values for metal samples cast after ultrasonic treatment are much higher than those observed for the reference samples. The two left arrows in Figure 5 show the minimal observed differ-

ences. The next two arrows represent differences between mean values. The mean elongation increased maximally by about 11.5%, which makes it 1.72 times greater than that observed for the reference specimens.

3.4. Ultimate Tensile Strength (UTS) after sonication

In Table 2 the mean elongation before and after treatment is presented.

Table 3. Mean UTS before (UTS) and after (UTS') treatment.

	UTS [MPa] reference	UTS' [MPa] after treatment	UTS'/UTS [*100%]
Ex1		79 ± 1.3	117%
Ex2	67.4 ± 2.6	72 ± 2.6	107%
Ex5 (*)		65.6 ± 4.5	98%

(*) degassing only, no grain refinement

The mean UTS before and after treatment was greater than the reference set increasing from about 7% to 17%. The metal cast in the experiment resists without permanent damage a pressure greater of about 12 MPa than the reference samples. To help understand these results, the Weibull distribution was fitted into the UTS data. Weibull plots of ultimate tensile strength (UTS) data of the castings have been presented in Figure 6.
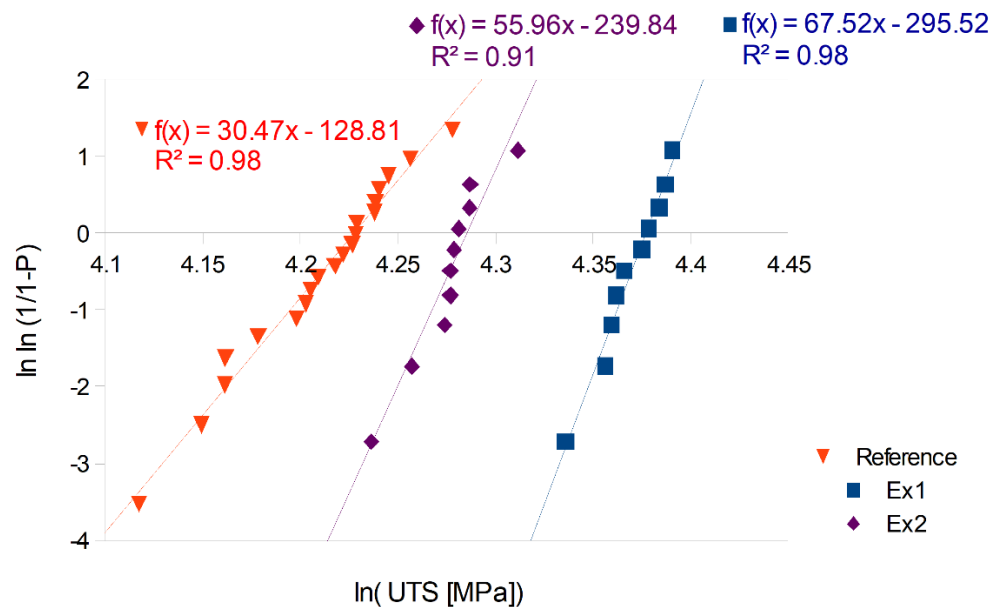

Figure 6. Weibull modulus established by the linear regression.

From the regression line equations, the Weibull modulus (m) of the reference set equals m_0=30.5. After treatment this modulus increased to m_1=67.5 in Ex1 and m_2=56.0 in Ex2. The data were fitted to Weibull distributions of m_1 and m_2 (and calculated scale pa-

rameters) and the curves of the Weibull probability plots have been presented in Figure 7.
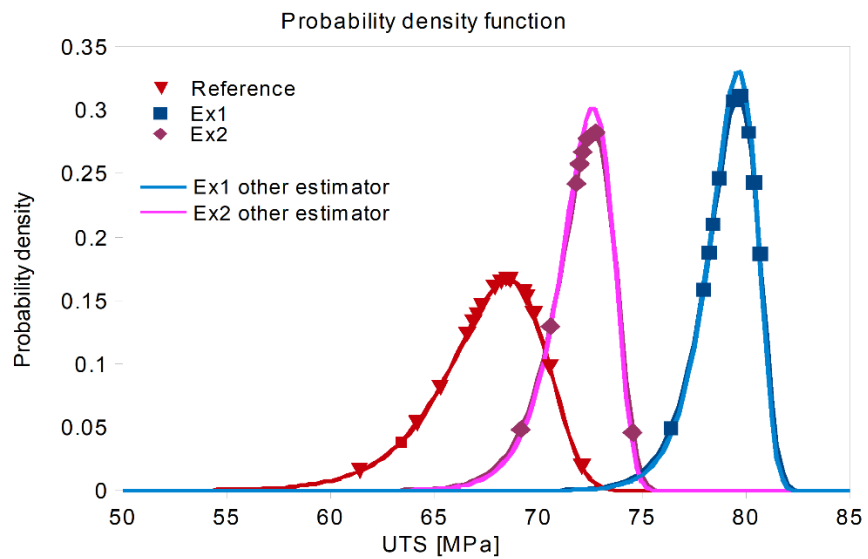

Figure 7. Probability density function (Weibull curve) of reference data versus results of both ultrasound treatments based on UTS measurements. The data points are overlayed on the calculated distribution indicated in Figure 6. Two lines labelled as "other estimator" show the other possible distribution, calculated with another estimator, as will be discussed further (method 3 at Table 4).

The shape of the distribution curve attributed to data from Experiment 1 shows that the expected scatter of the results was much smaller than that for the reference set. This is indicated by the narrower Weibull curve governed by the shape parameter (m, also known as the Weibull modulus). Results of Experiment 2 are better than those observed without treatment and the Weibull curve is also "narrow". Changing the estimators does not change the Weibull distribution significantly (see Section 4.3).

3.5. The stress-strain curves.

Figures 8 and 9 present the stress-strain curves for all specimens including both reference and treated (Ex1 and Ex2) metal.
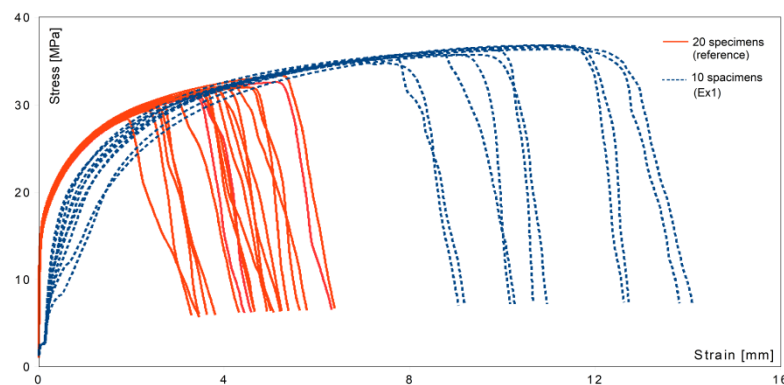

Figure 8. The stress versus the nominal strain curves for the specimens from the reference set and experimental (Ex1) set.

In Figure 8, the failure region for the reference set is observed at much lower values of strain, and the maximum stress which they hold out is higher than for untreated metal. Toughness, the ability of a material to absorb energy and plastically deform without fracturing, is defined by the area under the stress-strain curve [41]. The area under any of the experimental lines is larger than under the reference lines. The toughness of the material after ultrasound treatment in Ex1 is much higher than for the non-processed samples what is a good prediction for future engineering applications.
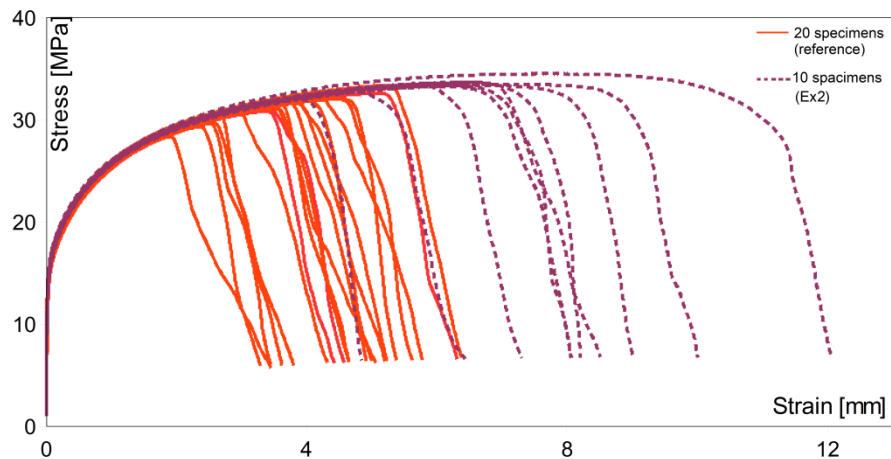

Figure 9. The stress versus the nominal strain curves for the specimens from the reference set and experimental (Ex2) set.

In the case of Ex2, the failure in most cases happened much later than for reference test bars. Two specimens break out earlier. This can be caused by other effects, as porosity or entrained oxide films. The overall effects of ultrasonic processing are positive and prove the efficacy of the contactless technique. The toughness of the material is also significantly improved. For most cases, the area under the curves is much bigger than recorded for the untreated metal. The variability between both experiments can be attributed to slightly different processing conditions, that are manually controlled. It is necessary to develop a feedback mechanism continuously adjusting the coil frequency for resonance and an accurate pressure monitoring system to control conditions more precisely in an industrial situation.

4. Discussion

4.1. Dataset validity

Before comparing the results a Students t-test was performed to decide if separately cast test-bars could be treated as coming from the same distribution. The first check confirmed that all samples produced as reference test-bars (obtained from two separate castings with repeated conditions) belonged to the same Weibull distribution and could be presented as one dataset (red triangles in Fig 6). The same test made for both experiments excluded the possibility that the data from Ex1 and Ex2 belonged to the same Weibull distribution. Results of that test (for Ex1 and Ex2) are shown in Figure 10.
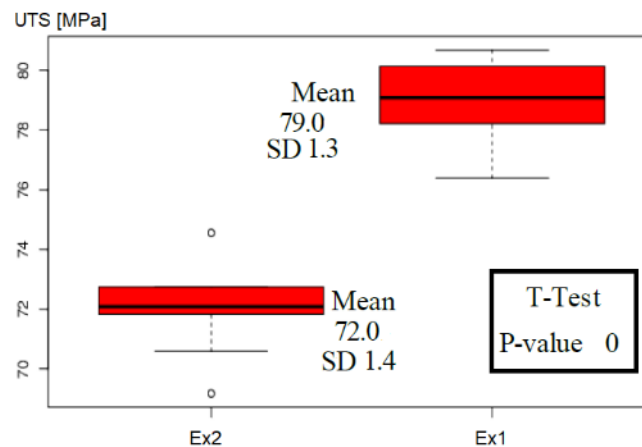
Figure 10. Results of 2 sided t-test of UTS measurements showing that Ex1 and Ex1 do not follow the same distribution. The test is done with 95% confidence.

The minimum p-value to accept the hypothesis that both experiments came from the same distribution was p=0.05 (5%), so for our data, the test rejected this hypothesis. The results of the t-test confirmed that the results of each experiment must be presented separately (Figure 6). At this moment, we have to rely only on 10 measurements of the strength produced in each experiment. The error bound up with that procedure will be further discussed.

4.2. Regression validity

One method allowing us to check the regression method validity is by observing the R^2 value. There exists a minimum value of R^2 to accept the fit of the data to the Weibull distribution as calculated by the linear regression method [37]. When the sample size is equal to 20, the minimum R^2 value is 0.894, and the R^2 value must be over 0.855 for n=10. In Figure 6 the value of R^2 is presented and the fit of lines found by regression was good enough to accept all the presented data. For the elongation data the fit was not good enough to present the Weibull modulus found by regression.

4.3. Validity of comparison between distributions

Even considering the R^2 test, the smaller sample size in the Weibull analysis resulted in an increased error [39]. To check if the results of the experiments (blue squares and purple diamonds in Figures 6 and 7) can be compared with the reference data (red triangles in Figures 6 and 7), we need to refer to the confidence intervals published earlier [34].

Comparison between two distributions (with known m and m') of sizes N=20 and N'=10 is possible with 95% of confidence if [40]:

$$1.889 < m'/m < 2.434.$$

For experiment 1 the $m'/m = m_1/m_0 = 2.216$. Because this value is inside the confidence interval given above, there is 95% confidence in comparing the Weibull moduli of both of these distributions.

For experiment 2 the $m'/m = m_2/m_0 = 1.837$ so we can compare it with the reference results with 90% confidence (where the confidence interval starts for $1.695 < m'/m$ as given at [40]).

Thus, even taking into account the errors we can confirm the quality improvement for both treatments with over 90% confidence.

4.4. Validation of used estimators

Fitting the correct distribution when the sample size is small should be done with the correct method. Several proposed estimators [38,40,42,43] and weighted linear regression [44,45] has been validated for Ex1 and Ex2. Results of the Anderson-Darling goodness-of-fit test are presented in Table 4.

Table 4. Anderson-Darling (AD) goodness of fit test for *m* calculated by unweighted linear regression (LR) or weighted linear regression (WLR) with different estimators. Already presented values are marked by the bold font.

No	Method	Used estimator	Estimated m from UTS data		AD test result (p-value)		Approach ref.
			Ex1	Ex 2	Ex1	Ex 2	
1	LR	P= (i-0.5) / n	71.7	59.6	0.99	0.67	[42]
2	LR	P= (i-0.348) / (n+0.19)	**67.5**	**56.0**	0.99	0.64	[38]
3	LR	P= (i-0.44) / (n+0.12)	69.7	57.8	0.91	0.67	[43]
4	WLR	P= (i-0.5) / n	59.6	56.3	≤0.05	0.66	[44,45]

.

The Anderson-Darling test rejects the dataset if the value $p \leq 0.05$. It simply means that, with 95% confidence, the data do not follow the chosen distribution. Both tested datasets show a good fit, with the p-value being on the extraordinary level of 0.99 for Ex1 validating previous analysis.

From Table 4, we can also conclude that the alteration of the estimators is not necessary, and the Anderson-Darling test is not showing significant differences between all the tested methods.

4.5. Expected error

To make further analysis easier, we round the m-values. For experiment 1 (see Table 4) the Weibull modulus is close to m1=68 and for experiment 2 m2=56. The mean values of the elongation and UTS after treatment (Table 2 and 3) prove that - even accounting for maximum error, both experiments improved the quality of the processed metal.

One can query the exact expected error in the established value of the Weibull modulus. The goodness of fit results can indicate that the chosen distribution was fitted correctly, even if based on a small number of measurements. To be more precise in the error estimation, we consider the estimated value for Ex1. By the computer simulation, the standard deviation and confidence intervals are calculated and shown in published research [38,40,45]. The error found is about 33% when only 10 test-bars are used [38,45]. For confirmation of that value, the results of computer simulation with 50 000 cycles were used to estimate the bias and the error (the standard deviation of the mean Weibull modulus calculated by different methods). The results have been presented in Table 5.

Table 5. The bias and the error comparison for methods (as in Table 4) used to estimate the Weibull modulus.

	Method	n	M	M'	Bias (M'/M)	Standard deviation (M')
Ex1	1			71.94	1.05	32.5%
	2	10	68	68.57	1.01	32.2%
	3			70.71	1.03	32.4%
Ex2	1			59.49	1.06	32.3%
	2	10	56	56.07	1.00	32.5%
	3			57.71	1.03	32.6%
Reference set	(*)	20	31	31.49	1.02	21.8%

(*) as in introduction for n=20

As we can see, the simulation results confirmed, that the expected error was about 33% when 10 samples are used. By increasing the number of measurements to 20 (a common procedure) this error was decreased by 10%. The most unbiased method is number 2, used in previous calculations for Ex1 and Ex2 (Figures 6,7).

Let us consider the worst-case scenario for Experiment 1. If the $m_1=68$ is overestimated by 33%, we will get the minimum value of Weibull modulus close to 46. This value is still significantly higher than was observed for the reference samples, equal to 31 - which is treated as given with sufficient certainty due to the higher number of data taken for calculations. Also, m is often between 10 and 30 for gravity-filled castings [32] and the value $m_0=31$ obtained without ultrasonication, seems to be reliable and is not expected to be much higher.

Experiment 2 also showed improvement of the metal quality, which supports the hypothesis about the significant improvement in Ex1. In that case, if the error will be maximal, the value will go down to about 40 which still can be seen as an improvement in the metal quality.

The mechanical properties, according to the Hall-Patch equation, are expected to be improved as the grain size decreases. Using the prediction from Figures 2 and 3 we can expect a better improvement of metal quality in Ex1 than in Ex2. Those changes are reflected in the calculated Weibull modulus values – the highest value of 68 for Ex1 (with small scatter of data, the small error in Table 2) and a smaller value of 56 for Ex2. The fact of gradual changes of m, according to the grain size, can be treated as another validation of established m. Thus, the expected error is below the maximum possible value.

The Weibull modulus of UTS for good quality aerospace castings is expected to be between 50-100 [32]. The m values characterising the processed alloys presented here are fulfilling those conditions.

4.6. Role of degassing and structure changes in metal straightening

Two measurable changes can be discerned due to sonication of the melt. The first one concerns the gas content, the second the grain size, reflecting changes on interfaces (forced wetting, undercooling, dispersion etc.). To find an answer as to which effect is dominant in the quality improvement obtained by the ultrasound, we need to recall the results of Ex5 (Tables 2,3).

The dataset for Ex5 was produced following treatment by the contactless sonotrode in the setup, where the number of collapsing bubbles was not sufficient to cause grain refinement. In other words, most of the bubbles created oscillated in size but did not burst. Due to the lack of shock wave emissions, the expected de-agglomeration and particle dispersion could not happen so we have not observed grain size reduction. Instead, processing by the contacless sonotrode caused degassing at the level of $0.06cm^3/100g$, without noticeable grain size change; this effect on its own did not improve the metal strength or elongation. Similar processing, with the same level of the gas removed during treatment followed by grain refinement, improved the metal properties significantly.

Thus, the main mechanism involved in the metal strengthening observed in Ex1 and Ex2 is caused by a grain size decrease rather than a decreased gas content. As a conclusion it is necessary to achieve full cavitation, at near-resonant frequency, to cause changes at the interface causing effective de-agglomeration and dispersion.

5. Conclusions

1. Contactless sonication provided significant changes in the observed microstructure of the cast alloy, decreasing the grain size by up to 48%.
2. The treatment is followed by a gas content decrease of up to $0.11 \, cm^3/100g$.
3. Ultrasonificated melts after casting exhibit improved ductile properties, the percentage of elongation increased maximally 1.7 times (from 16% to 28%).
4. The processed alloy shows a great improvement in strength. The mean UTS was increased by about 17%. This was followed by changes in the calculated Weibull modulus from 31 to 68. Even taking into account a maximum possible error, the quality of the metal after treatment has been significantly improved.

References

1. Bruna, M.; Galčík, M. Casting quality improvement by gating system optimization. Arch. Foundry Eng. 2021, 1, 132–136.
2. Dojka, R.; Jezierski, J.; Tiedje, N.S. Geometric Form of Gating System Elements and Its Influence on the Initial Filling Phase. J. of Materi Eng and Perform 2019, 28, 3922–3928.
3. Uludağ, M.; Gurtaran, M.; Dispinar, D. The Effect of Bifilm and Sr Modification on the Mechanical Properties of AlSi12Fe Alloy. Arch. Foundry Eng. 2020, 3, 99–104.
4. Abramov, O.V. Crystallization of metals in ultrasonic field, Science-Moscow 1972.
5. Eskin, G.I. Ultrasonic treatment of molten aluminum, Metallurgiya-Moscow 1965.
6. Eskin, G.I.; Eskin, D.G. Ultrasonic treatment of light alloy melts, 2nd ed.; CRC press: Boca Raton, USA, 2014; pp. 75-98.
7. Eskin, D.G.; Tzanakis, I.; Wang, F.; Lebon, G.S.B.; Subroto, T.; Pericleous, K.A.; Mi, J. Fundamental studies of ultrasonic melt processing. Ultrason Sonochem 2019, 52, 455-467.
8. Vives, C. Grain refinement in aluminum alloys by means of electromagnetic vibrations including cavitation phenomena, JOM-e 1998, 50(2).

9. Bojarevics, V.; Djambazov, G.S.; Pericleous, K.A. Contactless Ultrasound Generation in a Crucible. Metall Mater Trans A 2015, 46, 2884-2892.

10. Pericleous, K.A.; Bojarevics, V.; Djambazov, G.; Dybalska, A.; Griffiths, W.D.; Tonry, C.E.H. Contactless Ultrasonic Cavitation in Alloy Melts. Materials 2019, 12, 3610-3622.

11. Tonry, C.E.H.; Djambazov, G.; Dybalska, A.; Griffiths, W.D.; Beckwith, C.; Bojarevics, V.; Pericleous, K.A. Acoustic resonance for contactless ultrasonic cavitation in alloy melts. Ultrason Sonochem 2020, 63, 104959-104971.

12. Eskin, G.I. Cavitation mechanism of ultrasonic melt degassing, Ultrason Sonochem 1995, 2, S137-S141.

13. Eskin, D.G. Overview of Ultrasonic Degassing Development. In: Light Metals 2017; Ratvik, A., Eds.; Springer: Cham, Switzerland, 2017, pp. 1437-1443.

14. Campbell, J. Chapter 6 - Gas porosity. In: Castings, 2nd ed.; Campbell, J., Eds.; Butterworth-Heinemann: Oxford, UK, 2003, pp. 178-204.

15. Leighton, T.G.; Walton, A.J.; Pickworth, M.J.W. Primary bjerknes forces. Eur. J. Phys 1990, 11, 47-50.

16. Khavari, M.; Priyadarshi, A.; Hurrell, A.; Pericleous, K.A.; Eskin, D.G.; Tzanakis, I. Characterization of shock waves in power ultrasound. J. Fluid Mech. 2021, 915 (R3), 1-14.

17. Priyadarshi, A.; Khavari, M.; Subroto, T.; Conte, M.; Prentice, P.; Pericleous, K.A.; Eskin, D.G.; Durodola, J.; Tzanakis, I. On the governing fragmentation mechanism of primary intermetallics by induced cavitation. Ultrason Sonochem 2021, 70, 105260-105276.

18. Fan, Z.; Wang, Y.; Xia, M.; Arumuganathar, S. Enhanced heterogeneous nucleation in AZ91D alloy by intensive melt shearing. Acta Mater 2009, 57, 4891-4901.

19. Wang, F.; Eskin, D.G.; Connolley, T.; Wang, C.; Koe, B.; King, A.; Reinhard, C.; Mi, J. In-situ synchrotron X-ray radiography observation of primary Al2Cu intermetallic growth on fragments of aluminium oxide film, Mater. Lett. 2018, 213, 303-305.

20. Li, H.T.; Wang, Y.; Xia, M.; Zuo, Y.; Fan, Z. Harnessing oxides in liquid metals and alloys. In: Solidification Science and Technology, Fan, Z., Stone, I., Eds.; Brunel University Press: London, UK, 2011; pp. 93-110.

21. Lee, S.B.; Kim, Y.M. Direct observation of in-plane ordering in the liquid at a liquid Al/α-Al2O3 (1102) interface. Acta Mater 2011, 59, 1383-1388.

22. Wang, F.; Tzanakis, I.; Eskin, D.G.; Mi, J.; Connolley, T. In situ observation of ultrasonic cavitation-induced fragmentation of the primary crystals formed in Al alloys. Ultrason Sonochem 2017, 39, 66-76.

23. Pericleous, K.A.; Bojarevics, V.; Djambazov, G.; Dybalska, A.; Griffiths, W.D.; Tonry, C.E.H. The contactless electromagnetic sonotrode. In: Shape Casting 2019; Tiryakioğlu, M., Griffiths, W.D, Jolly, M., Eds.; Springer: Cham, Switzerland, 2019; pp. 239-252.

24. Tonry, C.E.H.; Djambazov, G.; Dybalska, A.; Bojarevics, V.; Griffiths, W.D.; Pericleous, K.A. Resonance from contactless ultrasound in alloy melts. In Light Metals 2019; Springer: Cham, Switzerland, 2019; pp. 1551–1559.

25. Pericleous, K.A.; Bojarevics, V.; Djambazov, G.; Dybalska, A.; Griffiths, W.D.; Tonry, C.E.H. Alloy grain refinement by means of electromagnetic vibrations. In: Proceedings of the Liquid Metal Processing & Casting Conference 2019; Jardy, A., Mitchell, A., Ward, R.M., Eds.; TMS, LMPC: Birmingham, UK, 2019; pp. 507-516.

26. Pericleous, K.A.; W.D.; Beckwith, Bojarevics, V.; Djambazov, G.; Dybalska, A.; Griffiths, W.D.; Tonry, C.E.H. Progress in the development of a contactless ultrasonic processing route for alloy grain refinement. IOP Conf Ser.: Mater. Sci. Eng. 2020, 861, 012070-012078.

27. Campbell, J. Castings, 2nd ed.; Elsevier: London, UK, 2003; pp. 481-483.

28. Zok, F.W. On weakest link theory and Weibull statistics. J Am Ceram Soc. 2017, 100, 1265–1268.

29. Green, N.R.; Campbell, J. Statistical distributions of fracture strengths of cast Al7SiMg alloy. Mater. Sci. Eng. A 1993, 173, 261-266.

30. Byczynski, G.E.; Campbell, J. The Effects of Oxide Film Defects on the Strength and Reliability of 319 Alloy Castings. In: Advances in Aluminum Casting Technology II; Tiryakioğlu, M.; Campbell, J., Eds.; ASM: Clevland, OH, USA, 2002; pp. 65-75.

31. Mi, J.; Harding, R.A.; Campbell, J. Effects of the entrained surface film on the reliability of castings. Metall. Mater. Trans A 2004, 35, 2893-2902.

32. Campbell, J. Castings, 2nd ed.; Elsevier: London, UK, 2003; p. 303.

33. Ono, K. A Simple Estimation Method of Weibull Modulus and Verification with Strength Data. Appl. Sci. 2019, 9, 1575-1614.

34. Leighton, T. G. Acoustic Bubble Detection. II. The detection of transient cavitation. Environ. Eng. 1995, 8, 16-25.

35. Manoylov, A.; Lebon, G.S.B., Djambazov, G., Pericleous, K.A. Coupling of acoustic cavitation with DEM-based particle solvers for modeling de-agglomeration of particle clusters in liquid metals. Metall. Mater. Trans. A, 2017, 48, 5616-5627.

36. Murty, B.S.; Kori, S.A.; Chakraborty, M. Grain refinement of aluminium and its alloys by heterogeneous nucleation and alloying. Int. Mater. Rev. 2002, 47, 3–29.

37. Tiryakioglu, M.; Hudak, D. Guidelines for Two-Parameter Weibull Analysis for Flaw-Containing Materials. Metall. Mater. Trans. B 2011, 42, 1130-1135.

38. Tiryakioglu, M.; Hudak, D. Unbiased estimates of the Weibull parameters by the linear regression method. J Mater Sci 2008, 43, 1914-1105.

39. Tiryakioglu, M.; Hudak, D. On estimating Weibull modulus by the linear regression method. J Mater Sci 2007, 42, 10173-10179.

40. Hudak, D., Tiryakioğlu, M. On comparing the shape parameters of two Weibull distributions, Mater. Sci. Eng. A 2011, 528, 8028-8030.

41.   Askeland, D.R. The science and engineering of materials., Seventh ed.; Cengage Learning: Boston, MA, 2016; pp. 208-209.

42.   Weibull, W. A Statistical Distribution Function of Wide Applicability. J. Appl. Mech. 1951, 18, 293-297.

43.   Li, T.; Griffiths, W.D.; Chen, J. Weibull Modulus Estimated by the Non-linear Least Squares Method: A Solution to Deviation Occurring in Traditional Weibull Estimation. Metall Mater Trans A 2017, 48, 5516-5528.

44.   Datsiou, K.C.; Overend, M. Weibull parameter estimation and goodness-of-fit for glass strength data. Structural Safety 2018, 73, p. 29-41.

45.   Faucher, B.; Tyson, W.R. On the determination of Weibull parameters. J Mater Sci Lett 1988, 7, 1199-1203.